Dual-Polarized Multi-Resonance Antennas With Broad Bandwidths and Compact Sizes for Base Station Applications

HAI-HAN SUN (Student Member, IEEE), CAN DING (Member, IEEE),
HE ZHU (Member, IEEE), AND Y. JAY GUO (Fellow, IEEE)

Global Big Data Technologies Centre, Faculty of Engineering and Information Technology, University of Technology Sydney, Sydney, NSW 2007, Australia

CORRESPONDING AUTHOR: H.-H. SUN (e-mail: hannah.h.sun@outlook.com)

ABSTRACT In this paper, a novel design method for dual-polarized multi-resonance antennas is presented for base station applications. The radiator of the antenna is configured as cross-dipoles with four thin metal strips connected to the adjacent dipole arms. The attached strips create multiple current paths and introduce additional resonant points. As a result, the bandwidth of the antennas is broadened while maintaining a very compact size. Based on this working mechanism, two multi-resonance antennas are designed, fabricated, and tested. The antennas achieve bandwidths of 46.7% and 66.7% respectively, with excellent matching capabilities. The antennas also exhibit high port isolation levels and stable radiation performances. The promising wideband performances with compact physical sizes make the antennas highly suitable for the base station applications.

INDEX TERMS Bandwidth enhancement, dual-polarized antennas, multi-resonance antennas, compact configuration.
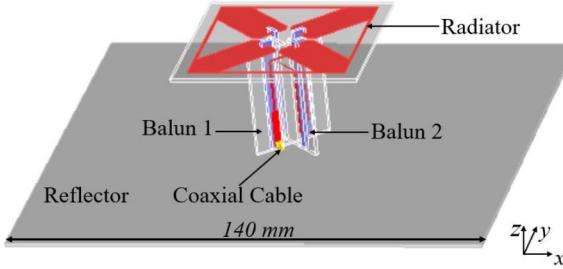
I. INTRODUCTION

CELLULAR base station antennas (BSAs) are critical components in wireless mobile communication systems. As the communication system evolves rapidly to the fifth generation (5G), antennas which can simultaneously support different standards and have high data capacity are in great demands. Multi-band antenna arrays with antenna elements at different bands closely interleaved with each other are one of the development trends for BSAs. This, however, placed stringent requirements on single antenna elements. For 3G/4G BSA elements, the industrial specifications include the ±45° dual-polarized radiation, wide bandwidth with good matching, high port isolation, and consistent radiation performances. In addition, practical considerations of reducing BSA's weight, wind load, and fabrication cost require the antenna element to have simple and robust antenna structures with compact sizes [1]. The small size of antenna elements also reduces the mutual coupling and cross-band interferences when applied in antenna arrays. Although there have been increasing research activities on BSA elements

recently [2]–[15], it is still a challenge to meet all these specifications simultaneously.

The cross-dipole antennas have been widely used in industry due to its straightforward structure and robust radiation performance. The radiator consists of a pair of dipoles oriented perpendicular to each other and backed by a reflector. Primitive cross-dipoles have the two sub-dipoles "isolated" from each other [2], [3]. The bandwidths they achieve are limited (less than 25%). To improve the bandwidth, tightly-coupled cross-dipoles (TCCDs) are developed [4]–[8]. The sub-dipoles are closely spaced to introduce strong mutual coupling and bring another resonance [4]–[6]. The resultant bandwidth could be enhanced to more than 45%. To further broaden the bandwidth, parasitic elements such as strips, disks, or loops are introduced on different layers near the radiators [9], [10]. The bandwidth can be enhanced to more than 60%, but at the expense of the antenna sizes and fabrication complexity.

The square-dipole-array antennas are another popular choice in base station applications [11]–[14]. The radiator

FIGURE 1. Perspective view of the multi-resonance antenna.

consists of four end-to-end dipoles forming a square loop. The four dipoles are excited simultaneously for each polarization. Wide bandwidth with stable radiation performances have been achieved, but the antennas usually occupy a large space, which limits their applications in antenna arrays.
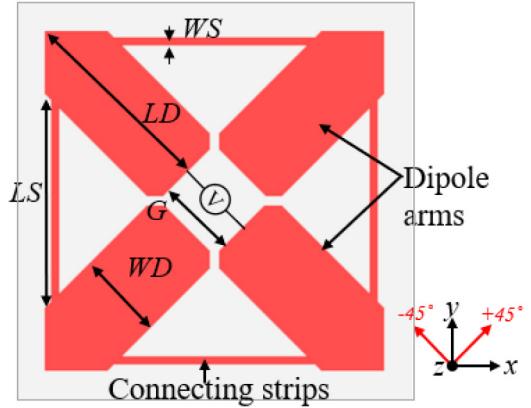
The challenging industrial requirement of the wide bandwidth and small antenna size remains an urgent issue to be addressed for BSAs. In this paper, we present a novel configuration of multi-resonance antennas to achieve a broad bandwidth with a very compact size. The radiator is formed by cross-dipoles with four thin metal strips connected to the adjacent dipole arms. The presence of metal strips brings in multiple current paths at different frequencies when the radiator is excited, thus introducing additional resonant points. By carefully optimizing the strips' dimensions, the additional resonant points can be tuned in the targeted band, resulting in a broadened bandwidth with good matching capability. The introduced strips do not increase the physical dimensions of the antenna, therefore, a compact antenna configuration can be guaranteed. Two dual-polarized multi-resonance antennas are designed and tested. The experimental results demonstrate that the antennas have wide operating bandwidths, high port isolations, stable radiation performances, and compact sizes, thus being highly suitable for base station applications.

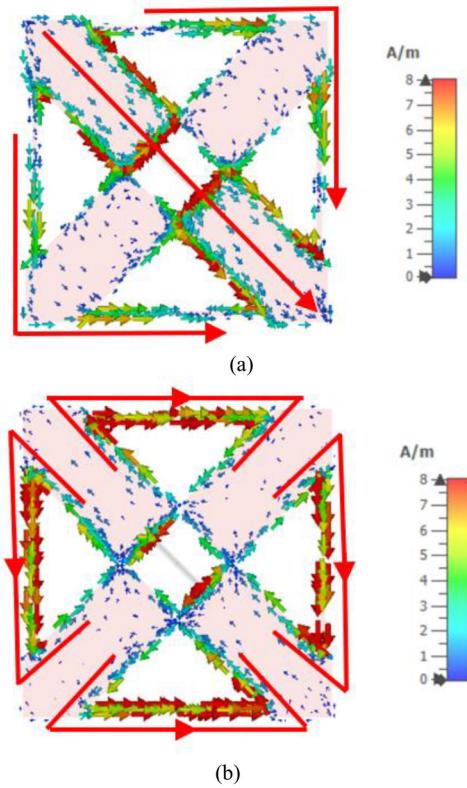## II. ANTENNA I: DUAL-POLARIZED MULTI-RESONANCE ANTENNA

Fig. 1 gives the perspective view of the dual-polarized multi-resonance antenna. The antenna consists of the multi-resonance radiator, two baluns for balanced feeding and impedance matching, and a reflector for directional radiation. Two coaxial cables are connected to two baluns to feed the antenna, with the outer conductors attached to the ground, and the inner conductors soldered on the transmission lines of baluns. The radiator is mounted above the reflector with a distance of 32 mm. The substrate used has a dielectric constant of 4.4, a loss tangent of 0.0025, and a thickness of 1.0 mm. The antenna is designed to cover 4G LTE bands from 1.71 GHz to 2.69 GHz.

A. WORKING MECHANISM OF THE MULTI-RESONANCE RADIATOR

A detailed view of the multi-resonance radiator is shown in Fig. 2. The radiator consists of two pairs of dipole arms

FIGURE 2. Configuration of the multi-resonance radiator.

FIGURE 3. Current distributions at the multi-resonance radiator at (a) 1.8 GHz and (b) 2.3 GHz.

perpendicularly positioned with each other, and four thin metal strips connected to adjacent dipole arms. By exciting each pair of dipole arms, +45° or −45°-polarized radiation can be obtained. The excitation for −45°-polarized radiation is shown in Fig. 2 as a demonstration.

To illustrate its working mechanism, the current distributions at 1.8 GHz and 2.3 GHz are shown in Figs. 3(a) and 3(b) respectively. At 1.8 GHz, there are three dominate current paths for −45°-polarized radiation. One path is along the driven arms, and two are along the connecting strips. The current distribution indicates that the radiator resembles an irregular-shaped three-arm folded
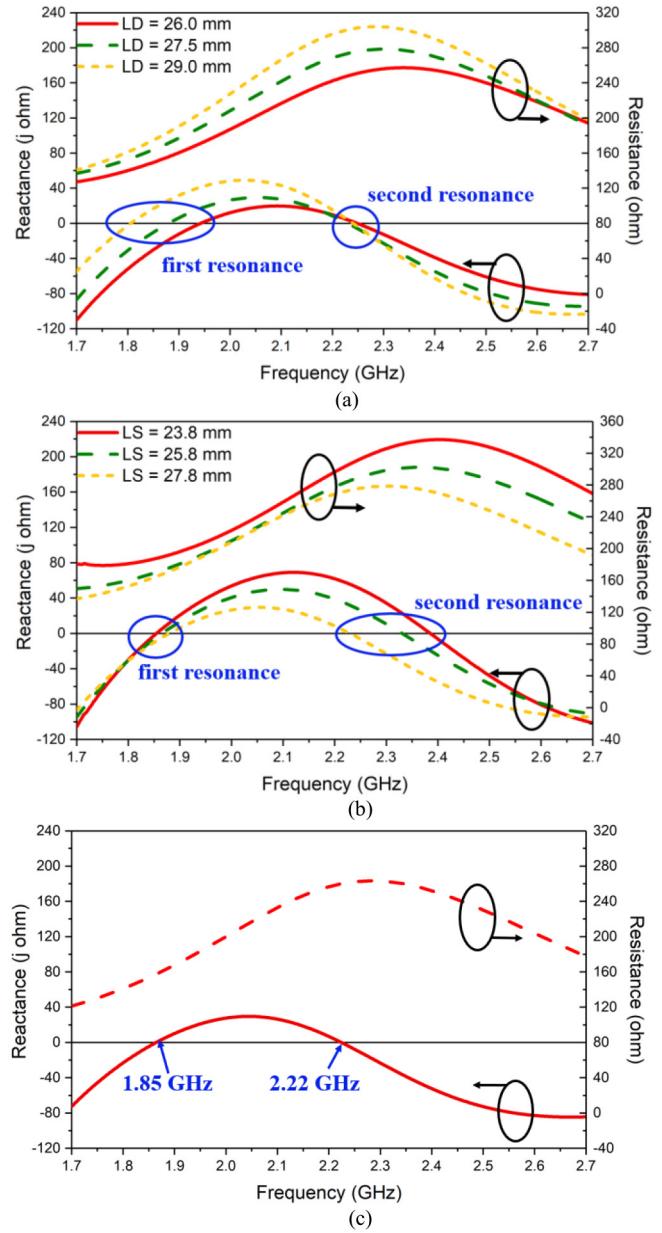
dipole. At 2.3 GHz, the currents are accumulated along the four connecting strips, with some extending to the side of dipole arms. The current distribution on each strip resembles the short dipole case, and the −45°-polarized radiation is achieved by the co-radiation of four current paths. The current distributions in Fig. 3 show that there are different dominant current paths at different frequencies on the same radiator's aperture, which helps to achieve multiple resonant points across a wideband with a compact configuration.

For the presented radiator, two parameters are directly related with the length of current paths, which are the length of dipole LD, and the length of the connecting strip LS. Therefore, these two parameters will have dominating impacts on the resonant points and the input impedances of the radiator. The input reactance and resistance with different LD and LS values are shown in Figs. 4(a) and 4(b). Obviously, there are two resonant points (reactance = 0) at all reactance curves, suggesting the radiator exhibits intrinsic dual-resonant property. As shown in Fig. 4(a), LD mainly influences the first resonant frequency at a lower band. Increasing LD moves the first resonant point to a lower frequency. As shown in Fig. 4(b), LS dominates the second resonant frequency at a higher band. Increasing LS decreases the second resonant frequency. These findings agree with the current distribution in Fig. 3 that LD and LS determine the length of current paths in the lower and higher bands, respectively.

It is also noted from Figs. 4(a) and 4(b) that the radiator has a relatively large resistance level, and that larger LD or smaller LS increase the resistance across the band. Therefore, appropriate values should be selected to make the radiator have desired resonance frequencies and reasonable resistance level for impedance matching. Other parameters of the radiator shown in Fig. 2 also have certain effects on the input impedance, and they are optimized in the design process as well. The optimized dimensions of the radiator are $LD = 27.5$ mm, $WD = 12$ mm, $LS = 29.7$ mm, $WS = 0.8$ mm and $G = 11$ mm. The input impedance is shown in Fig. 4(c). Across the targeted band from 1.7 GHz to 2.7 GHz, the radiator has two resonant frequencies at 1.85 GHz and 2.22 GHz with impedance varies from 125 Ω to 260 Ω. Later on, baluns are designed to match the radiator, which will be explained in the next section.

B. IMPEDANCE MATCHING OF THE MULTI-RESONANCE ANTENNA

To provide balanced feeds to the multi-resonance dipole radiators and transform the input impedance for matching, two baluns are designed following the guidelines in [14]–[16]. The circuit model of the balun are shown in Fig. 5(a). It consists of two line-transformers TL$_1$ and TL$_2$ and a series resonator formed by open circuit line (OCL) and short circuit line (SCL). The optimized values of the circuit components are listed in Table 1. The balun is implemented with microstrip structures, as shown in Fig. 5(b). The feed lines for the two baluns are arranged at slightly different heights

FIGURE 4. The influence of (a) dipole length LD, and (b) strip length LS on the input reactance and resistance of the multi-resonance radiator. (c) The input impedance of the radiator with optimized dimensions.

to avoid overlapping with each other. The optimized dimensions are marked in the figures. As the working mechanism and implementation of baluns have been thoroughly carried out in [14]–[16], we here only briefly describe the matching process of this multi-resonance antenna.

As shown in Fig. 5(a), the input impedance of the radiator is firstly connected with the series resonator, then transformed by two line-transformers and fed by a 50 Ω port. The transformed input reactance and resistance at different matching stages are plotted in Figs. 6(a) and 6(b) respectively. According to Fig. 6(a), the radiator has two resonant frequencies at 1.85 GHz and 2.22 GHz. The series resonator
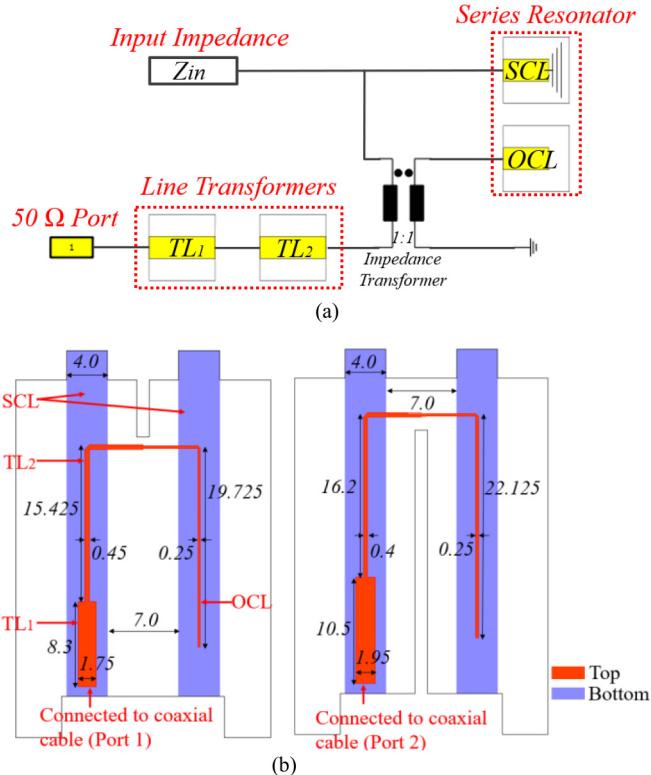
(a)

(b)

FIGURE 5. (a) Circuit model, and (b) microstrip realization of the baluns.

TABLE 1. Optimized values for circuit components in baluns.

Components	Impedance (Ω)	Length (mm)
SCL	500	45.14
OCL	131.58	45.14
TL$_1$	55.56	13.64
TL$_2$	98.89	34.21

(a)

(b)

FIGURE 6. (a) Input reactance and (b) input resistance of the antenna at different stages.

FIGURE 7. Matching results of the antenna with circuit balun and microstrip balun.

FIGURE 8. Fabricated prototype of the dual-polarized multi-resonance antenna.

introduces another resonant point at 2.46 GHz and alleviates the fluctuation of reactance across the band. The series resonator has little effects on first two resonant points. The line-transformers bring the fourth resonant point at 2.67 GHz, and move the first three points to 1.72 GHz, 2.04 GHz, and 2.41 GHz respectively. The variation of reactance is further smoothed with the line transformers, and the final reactance fluctuates around 0 across the targeted band. As shown in Fig. 6(b), the radiator alone has a quite high resistance within the designed band. The series resonator reduces the resistance at the high band from 2.2 GHz to 2.7 GHz. The line transformers as the key components transform the resistance to around 50 Ω. With the help of the baluns, the designed antenna achieves four resonant points and nearly 50 Ω resistance across the band from 1.7 GHz to 2.7 GHz. The matching results of the circuit model and realized microstrip model are shown in Fig. 7. The two results agree well with each other, and both are well matched to reflection coefficient < -15 dB from 1.69 GHz to 2.7 GHz.
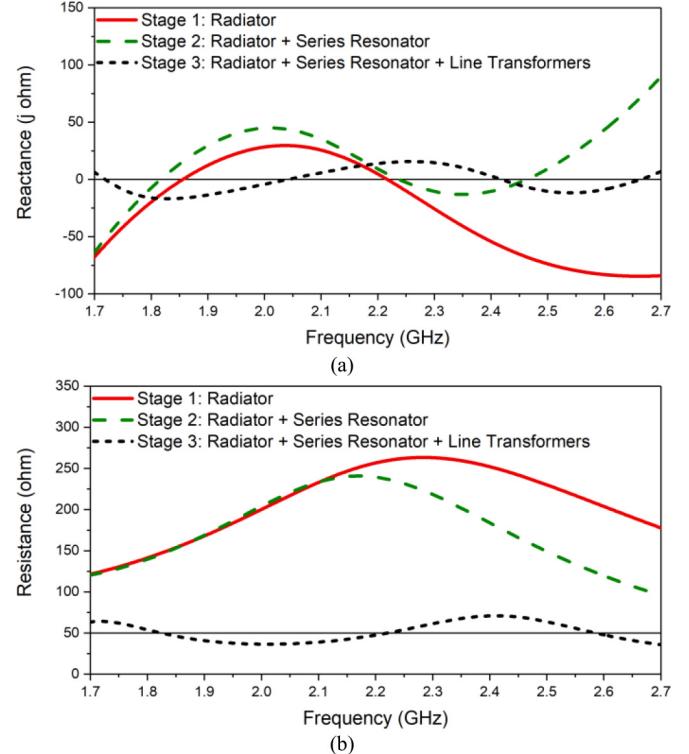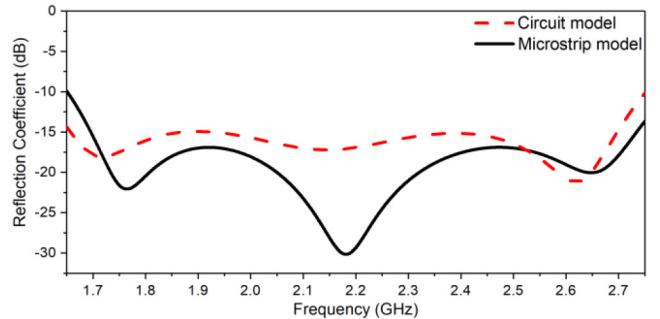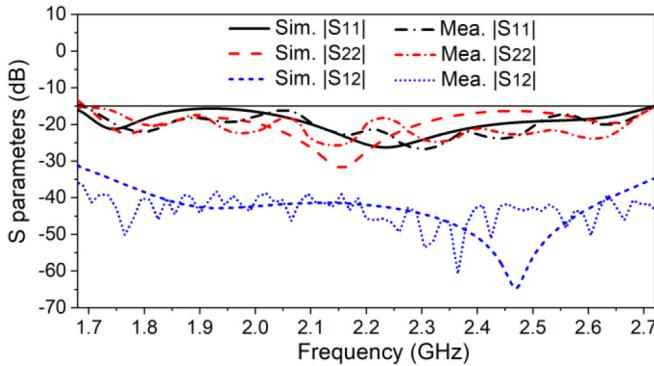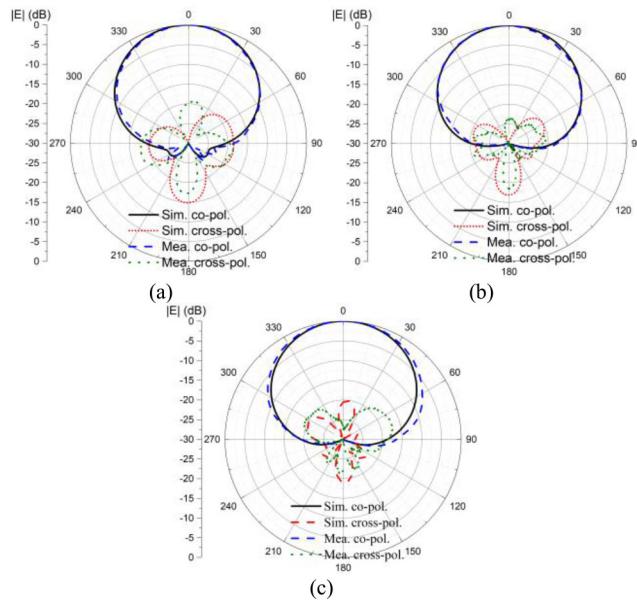
C. EXPERIMENTAL RESULTS

The dual-polarized multi-resonance antenna has been fabricated and tested. The fabricated prototype is shown in Fig. 8. The S-parameters of the antenna are shown in Fig. 9.
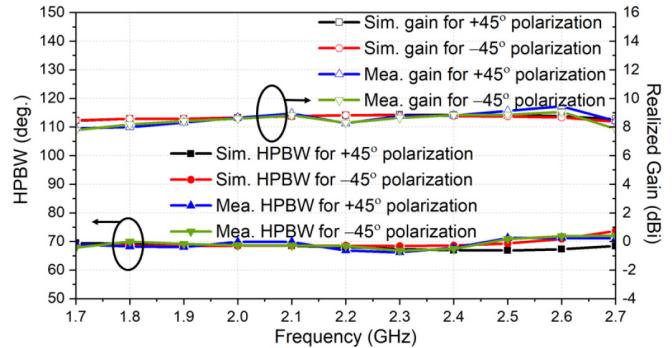
FIGURE 9. Simulated and measured S-parameters of the dual-polarized multi-resonance antenna.

FIGURE 11. Simulated and measured HPBW and realized gain of the dual-polarized multi-resonance antenna.

FIGURE 10. Horizontal radiation patterns of +45°-polarized radiation of dual-polarized multi-resonance antenna at (a) 1.7 GHz, (b) 2.2 GHz, and (c) 2.7 GHz.

The simulated and measured results are in good agreement. The results demonstrate that the antenna has a bandwidth of 46.7% from 1.69 GHz to 2.72 GHz with reflection coefficients less than −15 dB. Across the band, the measured $|S_{21}|$ is less than −35 dB, which guarantees a very high isolation level between the two ports. The radiation patterns in the horizontal plane (xz-plane) are shown in Fig. 10. The measured results agree well with the simulated ones, and the patterns are symmetrical and stable across the wide band. For the cross-polarization discrimination (XPD), the simulated results are > 22.5 dB at boresight, and > 9 dB within ±60° coverage, whereas the measured results are >19 dB at boresight, and > 10 dB within ±60° coverage. The simulated and measured half-power beamwidth (HPBW) and gain results are shown in Fig. 11. With a flat metal reflector, the antenna has very stable radiation patterns with horizontal HPBW of 68.7° ± 2.5° for the two polarizations. The realized gain is 8.6 ± 0.9 dBi.

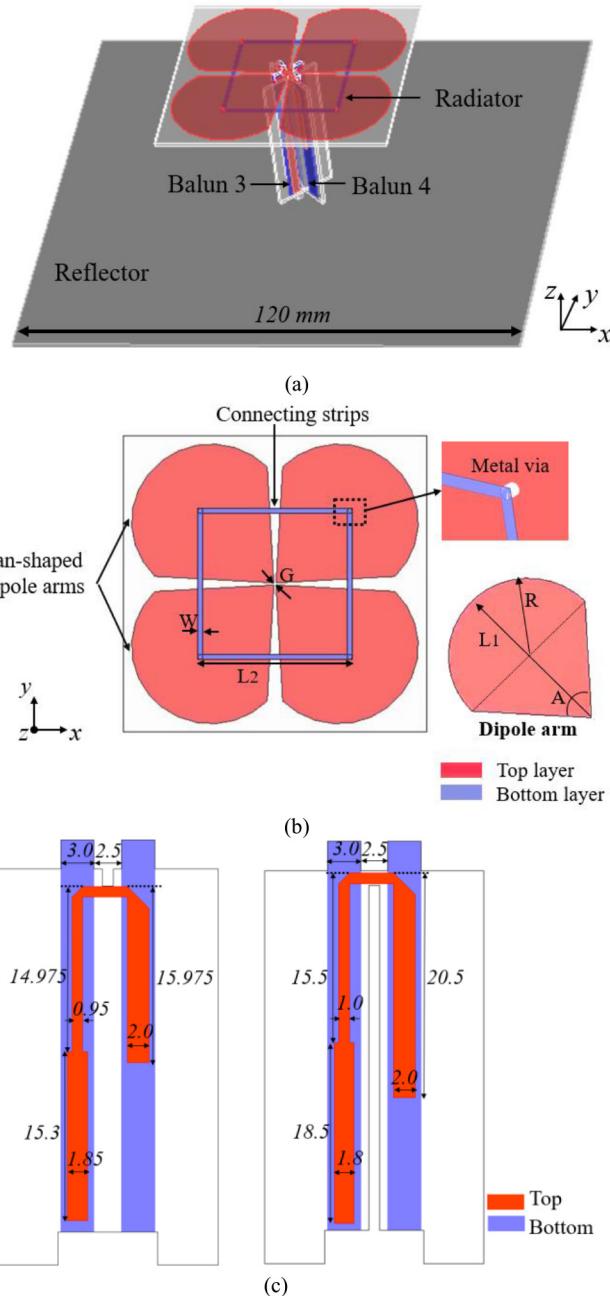## III. ANTENNA II: DUAL-POLARIZED TIGHTLY-COUPLED MULTI-RESONANCE ANTENNA

As introducing strong mutual coupling between dipole arms can bring in another resonance [4]–[8], in this section, we present a tightly-coupled multi-resonance (TCMR) antenna to further broaden bandwidth of the dual-polarized antennas.

The configuration of the TCMR antenna is shown in Fig. 12. Same with the antenna I, this antenna consists of the radiator, two baluns, and a flat reflector. The radiator is mounted above the reflector with a distance of 34 mm.

A. CONFIGURATION AND THE WORKING PRINCIPLE OF THE TCMR RADIATOR
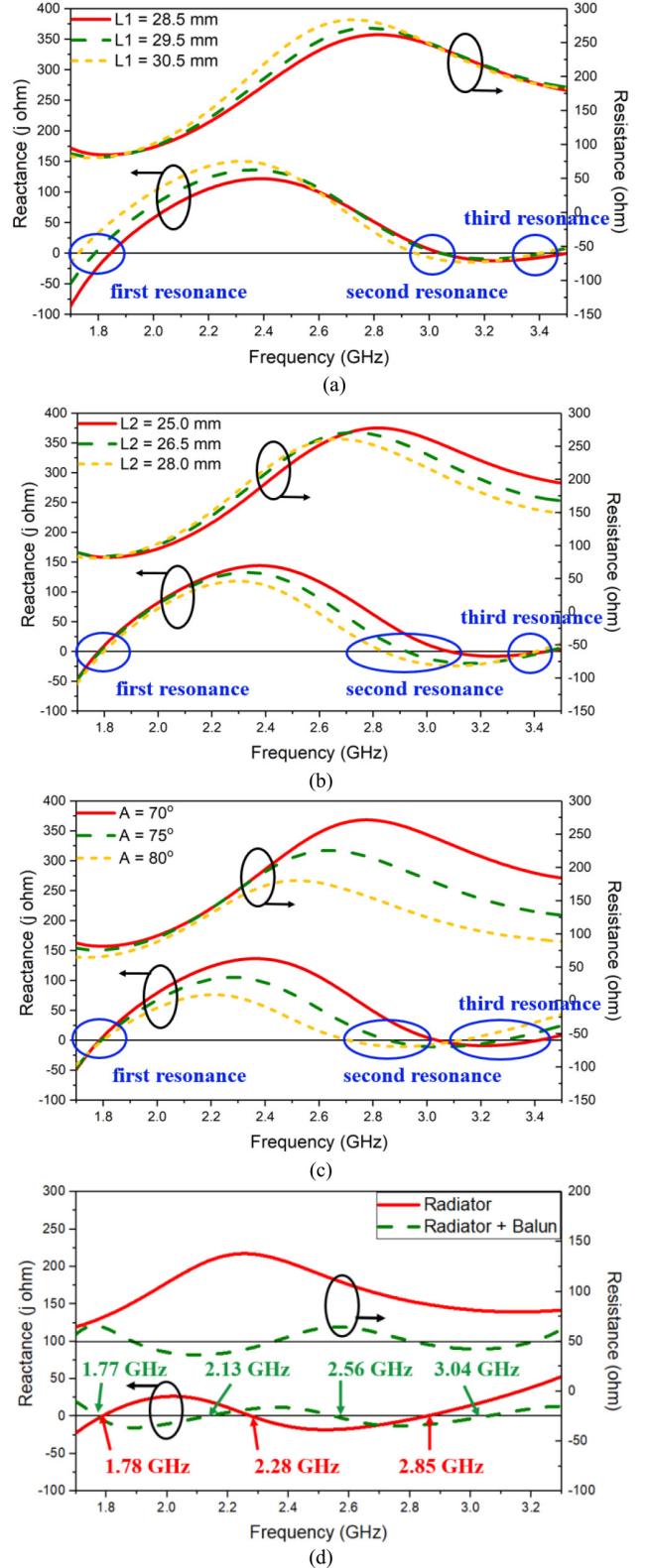
The detailed view of TCMR radiator is shown in Fig. 12(b). Fan-shaped dipoles are used as radiators and a strong mutual coupling is introduced by compactly arranging the antenna arms. Four metal strips are attached to the dipole arms to introduce additional current paths. The fan-shaped arm is composed of a triangular patch and a semi-circular patch. The relationship of the parameters L1, A, and R is $L1 = R \times (1 + 1/\tan(A/2))$. In this configuration, the four connecting strips are printed on the bottom layer of the substrate and connected to the dipole arms on the top layer using vias at the four corners. This double-layer arrangement is made because the TCCD arms are very fat, and if the connecting strips and the antenna arm are placed on the same layer, the connecting strip is too short to operate in the target frequency band.

The arm length L_1, the strip length L_2, and the angle A have large influences on the input impedance. The input impedance with different parameters are plotted in Figs. 13(a)-13(c). It can be noted that all the reactance curves have three resonant points, which indicates that the radiator has an inherent three-resonance characteristic. Figs. 13(a) and 13(b) show that the dipole length L_1 and the strip length L_2 mainly affects the first and the second resonant points, respectively. A larger L_1 results in a lower first resonant frequency, and a larger L_2 leads to a lower second resonant frequency. Fig. 13(c) shows that the first

FIGURE 12. (a) Perspective view of the RCMR antenna. (b) Detailed view of the TCMR radiator. (c) Detailed views of the two baluns.

FIGURE 13. The input resistance and reactance of the TCMR radiator with different values of (a) *L1*, (b) *L2*, (c) *A*, and (d) optimized dimensions. The transformed impedance of the antenna with the optimized balun is also shown in (d).

resonant point is insensitive to angle *A*, but the positions of the second and third resonant points vary greatly with different *A* values. Increase *A* increases the mutual coupling between dipoles, which moves the second and third resonant points to a lower frequency. Based on the analysis above, it can be concluded that the first resonance is generated by the dipole arms; the second resonance is produced by the combined effects of connecting strips and the mutual coupling between arms; the third resonance is introduced by the mutual coupling between dipole arms.

Figs. 13(a)-13(c) also shows the influences of the three parameters on the input resistance. Among them, the parameter *A* has the greatest influence. As shown in Fig. 13 (c),

FIGURE 14. Fabricated prototype of the dual-polarized tightly-coupled multi-resonance antenna.

TABLE 2. Optimized values for circuit components in baluns for TCMR antenna.

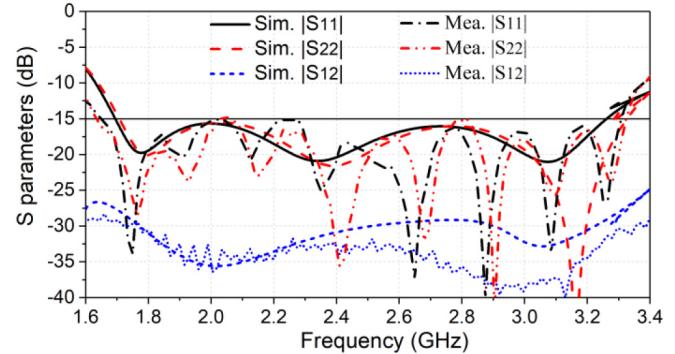| Components	Impedance (Ω)	Length (mm)
SCL	292	36
OCL	50	27.72
TL_1	55.56	19.2
TL_2	78.27	26.6

larger A dramatically reduces the resistance and alleviates the variation across the band, making the radiator easier to match.

The optimized dimensions of the radiator are $L_1 = 30.5$ mm, $A = 83.6°$, $L_2 = 28$ mm, $W = 0.8$ mm, and $G = 0.56$ mm. The substrate has a dielectric constant of 3.48, a loss tangent of 0.0037, and a thickness of 0.76 mm. The input impedance of the radiator with the optimized parameters is shown in Fig. 13(d). Three resonant points appear at 1.78 GHz, 2.28 GHz, and 2.85 GHz. The resistance varies from 60 Ω to 140 Ω from 1.7 GHz to 3.3 GHz. The three resonant points and the smooth resistance variation of the radiator make it possible to achieve broadband matching with a simple feeding structure.
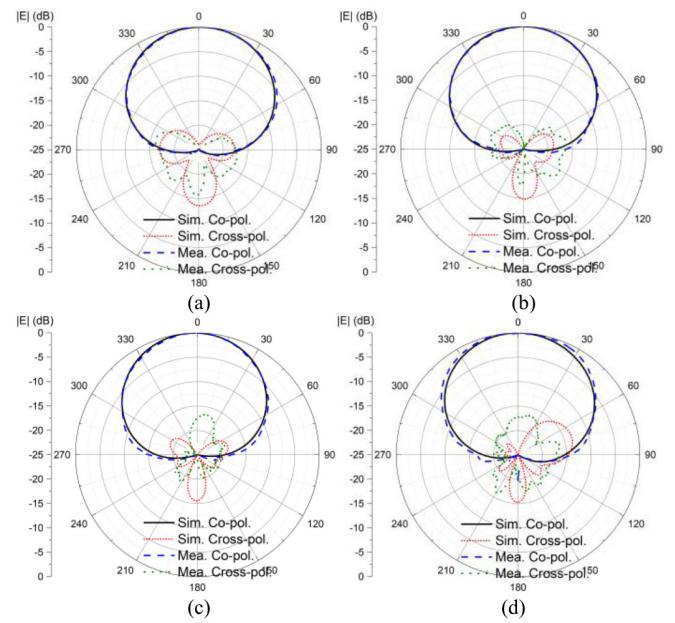
The feeding structure for the TCMR radiator is the same with the Antenna I, as shown in Fig. 5(a). The parameters of the circuit components are optimized for this case, and are listed in Table 2. Similar to the matching process of the Antenna I, the optimized feeding structure adds another resonant point, and transforms the resistance to around 50 Ω across the target band. The final input impedance of the TCMR antenna is shown as the dash lines in Fig. 13 (d). There are four resonant points at 1.77 GHz, 2.13 GHz, 2.56 GHz, and 3.04 GHz and the resistance varies around 50 Ω across the band from 1.7 GHz to 3.3 GHz. The antenna is well-matched across the band. The detailed configurations of the realized microstrip baluns are shown in Fig. 12(c).

B. EXPERIMENTAL RESULTS OF THE TCMR ANTENNA
The antenna is also fabricated and tested, as shown in Fig. 14. The antenna has a very compact size of $0.43 \times 0.43 \times 0.28\lambda_0^3$. λ_0 is the wavelength at the middle operating frequency 2.47 GHz. The simulated and measured S-parameters of the

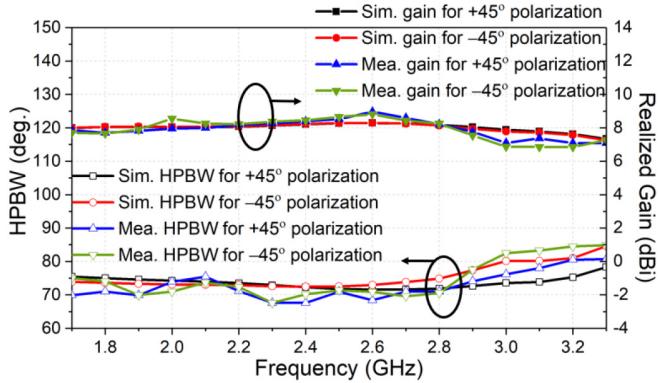**FIGURE 15.** S-parameters of the dual-polarized tightly-coupled multi-resonance antenna.

FIGURE 16. Radiation patterns of the dual-polarized tightly-coupled multi-resonance antenna at (a) 1.7 GHz, (b) 2.2 GHz, (c) 2.7 GHz, and (d) 3.2 GHz.

antenna is shown in Fig. 15. The antenna has a measured bandwidth of 66.7% from 1.65 GHz to 3.30 GHz with reflection coefficients for the two ports less than −15 dB. Across the band, the port isolation is above 28 dB. The simulated and measured radiation patterns are shown in Fig. 16. The patterns are very symmetrical and stable. The measured XPD is > 17 dB at boresight. The HPBW and gain results are shown in Fig. 17. The simulated and measured HPBWs of the radiation patterns vary within 78.0° ± 6.5°, and 76.0° ± 8.5° respectively for the two polarized radiation across the operating band. The realized gain is 7.9 ± 1.0 dBi.

C. COMPARISON AND DISCUSSION
The two designed antennas are compared with state-of-the-art BSAs, as listed in Table 3. The antennas are sorted by the bandwidth. The antenna size here is defined as the sizes of the radiators and the heights of the radiators above the reflectors. The size of the reflector is not considered as the elements are usually applied in arrays with a common

FIGURE 17. HPBW and gain of the dual-polarized tightly-coupled multi-resonance antenna.

TABLE 3. Comparison of antennas' performances.

Ref.	Size (λ_0^3)	BW	Isolation (dB)	HPBW
[3]	0.33×0.33×0.31	23.7%	25	63° ± 5°
[11]	0.49×0.49×0.23	23.7%	30	65.3° ± 1.2° *
[8]	0.42×0.42×0.26	45%	30	65° ± 5° *
[13]	0.50×0.50×0.21	45.2%	30	65° ± 4.5°
[14]	0.51×0.51×0.20	46.4%	28	66.5° ± 5.5°
Ant I in this work	0.34×0.34×0.23	46.7%	35	68.7° ± 2.5°
[4]	0.45×0.45×0.23	48%	22	62° ± 4° *
[9]	0.48×0.48×0.39	63%	30	60° ± 10°
	0.93×0.93×0.38	64%	30	70° ± 8°
Ant II in this work	0.43×0.43×0.28	66.7%	28	76° ± 8.5°
[10]	0.46×0.46×0.35	67%	30	65° ± 5° *

* The HPBW is measured with a shaped reflector.

large reflector for BSA applications. Compared with antennas with comparable bandwidth, such as Ant I with [8], [13], and [14], and Ant II with [9] and [10], the designed antennas have the smallest sizes. Compared with antennas with comparable antenna size, such as Ant I with [3], and Ant II with [4] and [8], the presented antennas have a much broader bandwidth. Note that the antenna presented in [8] is a similar tightly-coupled fan-shaped cross-dipole without connecting strips. The comparison of this antenna and Ant II verifies that the additional connecting strips help to enhance the bandwidth without increasing the electrical size of the antenna. In addition, the designed two antennas achieve comparable port isolation levels and HPBW variations. The comparison results demonstrate that the multi-resonance antennas presented in this work achieve broad operating bandwidths and compact configurations simultaneously without affecting other performance characteristics.

IV. CONCLUSION

In this work, a new design method of dual-polarized multi-resonance antennas is presented to broaden the bandwidth with 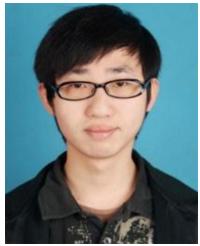a compact size. By connecting cross-dipole arms with four thin metal strips, different dominating current paths are created at different frequencies, and additional resonant points are introduced without increasing the physical size of the radiator. As a result, the antenna can achieve a broader bandwidth with a very compact and simplified configuration. As a demonstration, two dual-resonance antennas are presented. The realized two antennas have bandwidths of 46.7% and 66.7% respectively with very compact sizes. The isolation between two polarized ports are not affected, maintaining a high level above 28 dB. Experimental results show that radiation performances of the two antennas are stable across entire operating bands. The wideband coverage, consistent radiation performances, together with the compact and simple configurations make the two antennas highly suitable to be used in base station applications.

REFERENCES

[1] Z.-N. Chen and K.-M. Luk, *Antennas for Base Stations in Wireless Communications*, New York, NY, USA: McGraw-Hill, 2009.

[2] D. Su, D. Fu, T. N. C. Wang, and H. Yang, "Broadband polarization diversity base station antenna for 3G communication system," *J. Electromagn. Waves Appl.*, vol. 22, no. 4, pp. 493–500, 2008.

[3] D. Su, J. J. Qian, H. Yang, and D. Fu, "A novel broadband polarization diversity antenna using a cross-pair of folded dipoles," *IEEE Antennas Wireless Propag. Lett.*, vol. 4, pp. 433–435, Dec. 2005. [Online]. Available: https://ieeexplore.ieee.org/document/1545814

[4] H. Huang, Y. Liu, and S. Gong, "A broadband dual-polarized base station antenna with sturdy construction," *IEEE Antennas Wireless Propag. Lett.*, vol. 16, pp. 665–668, Mar. 2017. [Online]. Available: https://ieeexplore.ieee.org/document/7539335

[5] Z. Bao, X. Zong, Z. Nie, and S. Yang, "Design and discussion of a broadband cross-dipole with high isolation and low cross-polarisation utilising strong mutual coupling," *IET Microw. Antennas Propag.*, vol. 8, no. 5, pp. 315–322, Apr. 2014.

[6] Z. Bao, Z. Nie, and X. Zong, "A novel broadband dual-polarization antenna utilizing strong mutual coupling," *IEEE Trans. Antennas Propag.*, vol. 62, no. 1, pp. 450–454, Jan. 2014.

[7] C. Ding, H. Sun, R. W. Ziolkowski, and Y. J. Guo, "Simplified tightly-coupled cross-dipole arrangement for base station applications," *IEEE Access*, vol. 5, pp. 27491–27503, Nov. 2017.

[8] Y. Cui, R. Li, and H. Fu, "A broadband dual-polarized planar antenna for 2G/3G/LTE base stations," *IEEE Trans. Antennas Propag.*, vol. 62, no. 9, pp. 4836–4840, Sep. 2014.

[9] L. Wu, R. Li, Y. Qin, and Y. Cui, "Bandwidth-enhanced broadband dual-polarized antennas for 2G/3G/4G and IMT services," *IEEE Antennas Wireless Propag. Lett.*, vol. 17, no. 9, pp. 1702–1706, Sep. 2018.

[10] Y. Cui, L. Wu, and R. Li, "Bandwidth enhancement of a broadband dual-polarized antenna for 2G/3G/4G and IMT base stations," *IEEE Trans. Antennas Propag.*, vol. 66, no. 12, pp. 7368–7373, Dec. 2018.

[11] Y. H. Huang, Q. Wu, and Q.-Z. Liu, "Broadband dual-polarised antenna with high isolation for wireless communication," *Electron. Lett.*, vol. 45, no. 14, pp. 714–715, Jul. 2009.

[12] S.-G. Zhou, P.-K. Tan, and T.-H. Chio, "Low-profile, wideband dual-polarized antenna with high isolation and low cross polarization," *IEEE Antennas Wireless Propag. lett.*, vol. 11, pp. 1032–1035, Aug. 2012. [Online]. Available: https://ieeexplore.ieee.org/document/6286982

[13] H. Sun, C. Ding, T. S. Bird, Y. J. Guo, "A base station antenna element with simple structure but excellent performance," in *Proc. 3rd Aust. Microw. Symp.*, Feb. 2018, pp. 35–36.

[14] H. Sun, C. Ding, B. Jones, and Y. J. Guo, "A wideband base station antenna element with stable radiation pattern and reduced beam squint," *IEEE Access*, vol. 5, pp. 23022–23031, Oct. 2017.

[15] W. K. Roberts, "A new wide-band balun," *Proc. IRE*, vol. 45, no. 12, pp. 1628–1631, Dec. 1957.

[16] C. Ding, B. Jones, Y. J. Guo, and P.-Y. Qin, "Wideband matching of full-wavelength dipole with reflector for base station," *IEEE Trans. Antennas Propag.*, vol. 65, no. 10, pp. 5571–5576, Oct. 2017.

HAI-HAN SUN received the bachelor's degree in electronic information engineering from the Beijing University of Posts and Telecommunications, Beijing, China, in 2015, and the Ph.D. degree in engineering from the University of Technology Sydney, Australia, in 2019. She is currently a Research Fellow with the School of Electrical and Electronic Engineering, Nanyang Technological University, Singapore. Her research interests include the base station antennas and the ground penetrating radar.

CAN DING received the bachelor's degree in microelectronics from Xidian University, Xi'an, China, in 2009, and the Ph.D. degree from Macquarie University, Sydney, Australia, in 2015.

From 2012 to 2015, he was under the cotutelle agreement between Macquarie University and Xidian University. During this same period, he was also with Commonwealth Scientific and Industrial Research Organisation DPaS Flagship, Marsfield, Australia. From 2015 to 2017, he was an industrial-sponsored Post-Doctoral Research Fellow with the Global Big Data Technologies Centre, University of Technology Sydney, where he is currently a Lecturer. His research interest is in the area of base station antennas, reconfigurable antennas, phase shifters, and fibres for wireless communication and sensing.
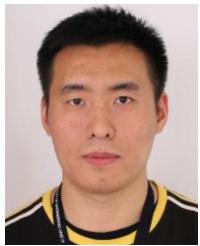
Dr. Ding is a recipient of the Australia Research Council Distinguish Early Career Researcher Award Fellow in 2020.

HE ZHU received the B.Sc. and M.Eng. degrees from the South China University of Technology, Guangzhou, China, and the Ph.D. degree in electrical engineering from the School of ITEE, University of Queensland, Brisbane, Australia. He is currently a Post-Doctoral Research Fellow with the Global Big Data Technologies Centre, University of Technology Sydney, Australia.

His research interests include development of passive and tunable microwave and mm-wave devices, radio frequency integrated circuits and systems, and beam-forming networks for antenna arrays.

Y. JAY GUO (F'14) received the bachelor's and master's degrees from Xidian University, China, in 1982 and 1984, respectively, and the Ph.D. degree from Xian Jiaotong University, China, in 1987.

He held various senior technology leadership positions with Fujitsu, Siemens, and NEC, U.K. In 2014, he served as the Director of CSIRO over nine years. He is a Distinguished Professor and the Founding Director of the Global Big Data Technologies Centre, University of Technology Sydney, Australia. He has published over 460 research papers including 250 journal papers, and holds 26 patents in antennas and wireless systems. His research interest includes antennas, mm-wave and THz communications, and sensing systems as well as big data technologies.

Dr. Guo has won a number of most prestigious Australian Engineering Excellence Awards in 2007 and 2012, and the CSIRO Chairman's Medal in 2007 and 2012, and was named one of the most influential engineers in Australia in 2014 and 2015. He has chaired numerous international conferences and served as guest editor for a number of IEEE publications. He is the Chair Elect of International Steering Committee and International Symposium on Antennas and Propagation. He was the International Advisory Committee Chair of IEEE VTC2017, the General Chair of ISAP2015, iWAT2014, and WPMC2014, and the TPC Chair of IEEE WCNC in 2010, and IEEE ISCIT in 2012 and 2007. He served as the Guest Editor of special issues on "Antennas for Satellite Communications" and "Antennas and Propagation Aspects of 60-90 GHz Wireless Communications," both in the IEEE TRANSACTIONS ON ANTENNAS AND PROPAGATION, the Special Issue on "Communications Challenges and Dynamics for Unmanned Autonomous Vehicles," in the IEEE JOURNAL ON SELECTED AREAS IN COMMUNICATIONS, and the Special Issue on "5G for Mission Critical Machine Communications," in the *IEEE Network Magazine*. He is a fellow of the Australian Academy of Engineering and Technology and IET, and he was a member of the College of Experts of Australian Research Council from 2016 to 2018.